

UC Davis

UC Davis Previously Published Works

Title

CoreView: fresh tissue biopsy assessment at the bedside using a millifluidic imaging chip

Permalink

<https://escholarship.org/uc/item/3678r52c>

Journal

Lab on a Chip, 22(7)

ISSN

1473-0197

Authors

Cooper, David J
Huang, Chuqin
Klavins, Dylan A
et al.

Publication Date

2022-03-29

DOI

10.1039/d1lc01142a

Peer reviewed



Cite this: *Lab Chip*, 2022, 22, 1354

CoreView: fresh tissue biopsy assessment at the bedside using a millifluidic imaging chip†

David J. Cooper,^a Chuqin Huang,^b Dylan A. Klavins,^c Mark E. Fauver,^c Matthew D. Carson,^c Farzad Fereidouni,^d Suzanne Dintzis,^e Csaba Galambos,^f Richard M. Levenson^d and Eric J. Seibel^{*a,c}

Minimally invasive core needle biopsies for medical diagnoses have become increasingly common for many diseases. Although tissue cores can yield more diagnostic information than fine needle biopsies and cytologic evaluations, there is no rapid assessment at the point-of-care for intact tissue cores that is low-cost and non-destructive to the biopsy. We have developed a proof-of-concept 3D printed millifluidic histopathology lab-on-a-chip device to automatically handle, process, and image fresh core needle biopsies. This device, named CoreView, includes modules for biopsy removal from the acquisition tool, transport, staining and rinsing, imaging, segmentation, and multiplexed storage. Reliable removal from side-cutting needles and bidirectional fluid transport of core needle biopsies of five tissue types has been demonstrated with 0.5 mm positioning accuracy. Automation is aided by a MATLAB-based biopsy tracking algorithm that can detect the location of tissue and air bubbles in the channels of the millifluidic chip. With current and emerging optical imaging technologies, CoreView can be used for a rapid adequacy test at the point-of-care for tissue identification as well as glomeruli counting in renal core needle biopsies.

Received 16th December 2021,
Accepted 29th January 2022

DOI: 10.1039/d1lc01142a

rsc.li/loc

Introduction

Histopathology and the technologies used to perform it have not changed significantly for over 75 years, with the exception of the development of immunohistochemistry in the 1980s, and *in situ* molecular tests in the last few decades.¹ Current histopathology practices are tissue destructive, labor-intensive, and costly, and take hours to days to complete. In addition, the traditional tissue preparation methods used in histopathology are not miniaturized nor optimized for needle biopsies, such as core (CNB) and fine needle biopsies (FNB), which have become the preferred biopsy technique for many organs due to their minimal invasiveness.² Millions of needle

biopsies are procured annually, prompting the need to automate and standardize their processing to support molecular diagnostic tests used for personalized medicine and precision therapy.

Needle biopsies have a significantly higher incidence of inadequacy, or the lack of an adequate sample of tumor for diagnostic assessment, compared to invasive surgical excisions because they sample small regions of tissue.³ Inadequate biopsies frequently lead to diagnostic delay, biopsy procedure repetition, and inconclusive histopathologic results. As a result, rapid on-site evaluation (ROSE) adequacy analysis has become increasingly relied upon to provide timely diagnostic and adequacy information from small needle biopsies with the least burden to the patient, the biopsy operator, and the hospital administration.² Touch preparation (TP) is the most common ROSE technique used on small needle biopsies to create cytologic samples, but it requires skilled manual steps and operators with cytopathology training. Furthermore, TP has limited utility for fibrous, cystic, and necrotic lesions.⁴ Moreover, cells are dislodged from the biopsy by physically rolling or squashing the tissue on a glass slide, potentially damaging the specimen and producing artifacts that disrupt downstream pathologic evaluation.

Additionally, ROSE techniques do not provide information about diagnostically relevant tissue architecture because they are cytologic, not histologic, interpretations. One

^a Department of Bioengineering, University of Washington, 3720 15th Ave NE, Seattle, Washington, USA. E-mail: eseibel@uw.edu

^b Department of Biomedical Engineering, State University of New York at Buffalo, 208 Bonner Hall, Buffalo, New York, USA

^c Department of Mechanical Engineering, University of Washington, 143 MEB, 3900 E. Stevens Way, Seattle, Washington, USA

^d Department of Pathology & Laboratory Medicine, University of Davis Health, 4400 V St, Sacramento, California, USA

^e Department of Laboratory Medicine & Pathology, University of Washington Medicine, 1959 NE Pacific St, Seattle, Washington, USA

^f Department of Pathology, University of Colorado Medicine, 13123 E 16th Ave, Aurora, Colorado, USA

† Electronic supplementary information (ESI) available: Supplemental.pdf contains all supplemental figures and tables. Supplemental videos are separate as Movie S1.mp4 and Movie S2.mov. See DOI: 10.1039/d1lc01142a

architectural feature that we chose to focus on was the number of glomeruli in renal CNBs. Glomeruli are routinely counted by a trained pathologist on-site using a basic light microscope to determine if there is an adequate number to provide a kidney disease diagnosis. The most notable problem associated with this procedure is the need to ensure enough glomeruli are present in the acquired biopsy. In a study that examined the risk of complications from renal biopsies over a 20 year span, it was found that each renal biopsy has a major complication rate of 3.9–6.5%.⁵ Therefore, it is important to limit the number of renal CNBs through immediate adequacy assessment.

To enhance rapid and accurate evaluation of CNBs to determine adequacy and avoid excess tissue sampling, we have developed a histopathology lab-on-a-chip device, named CoreView, based on a novel millifluidic system that automates the tissue handling process from needle acquisition to imaging. Preceded by modular microfluidic architectures in 2D and 3D, the millifluidic chip design is developed in modular format for the required steps of making a rapid tissue assessment on roughly 1 mm diameter CNBs.^{6,7} The millifluidic chip features sequential modules for biopsy removal from the procurement device, transport between modules, staining and rinsing, optical imaging, segmentation, storage, and removal. The CoreView system can be used with any crude or advanced optical microscope designed for thick-tissue 3D imaging. Fixation and optical clearing steps can also be included for deep tissue microscopic analysis being developed for slide-free volumetric histopathology.⁸ Our CoreView system is unique in the ability to rapidly and gently remove CNBs from side-cut needles. Furthermore, custom bidirectional pulsatile flows enable precise non-destructive bidirectional transport and staining of these fresh biopsies with the goal of performing ROSE adequacy in seconds and slide-free histology in minutes.

Experimental

Animal tissue models

All biopsies used for testing the CoreView chip and its components were acquired from resected organs obtained from recently euthanized female Yorkshire pigs. These pigs were undergoing trials for unrelated research in the UW Center for Industrial and Medical Ultrasound. Therefore, this project did not demand additional loss of life, outside of other research being conducted on campus, or raise additional ethical considerations or requirements.

3D printing, post-processing, and assembly of the CoreView chip

All 3D printed parts were printed using a form 3 (Formlabs, USA) low force stereolithography printer. Most parts were printed using standard clear resin (Formlabs), except for the biopsy segmentation elastomeric buffer which was printed using Elastic 50A resin (Formlabs). Computer-aided design

(CAD) models were developed using SolidWorks 2018 (SolidWorks Corporation, USA). All prints were made with the default 3D print parameters for each resin type and with auto-generated supports in the PreForm application (Formlabs). Prior to the removal of supports, all prints were washed in isopropyl alcohol (IPA) for six minutes to remove uncured photopolymer resin. Prior to post-curing, internal channels were flushed with IPA and then with compressed air to remove any uncured resin or debris and to identify problematic blockages. If successfully cleared using compressed air, the parts were post-cured using a manufacturer-recommended protocol in a FormCure (Formlabs) until fully hardened.

Aside from the channel ports on the sides of the chip, the only opening on the CoreView chip is the staining-and-imaging chamber. This opening is sealed after curing by using a double-sided adhesive [300LSE, 3M], laser cut around the opening, to attach a coverslip. This prevents the resin-based chip from obscuring or distorting the histopathologic image and is the only post-print modification to the CoreView chip.

LabVIEW millifluidics control

All CoreView millifluidics are controlled by a single LabVIEW 2020 (National Instruments, USA) program. This program controls the pumps and valves using dedicated custom drive electronics and a pair of data acquisition devices (USB-6002 DAQ, National Instruments). It also controls illuminations sources and captures camera image data. The current program is manually triggered to provide pulsatile flow, but a later version will automatically perform all CoreView functions.

Biopsy removal module design and testing

The most important feature of the CoreView histopathology on a chip is the automation because it avoids the need for human handling of fresh needle biopsies. Furthermore, removing the biopsy from its needle is one of the more challenging tasks because if done incorrectly, it can distort or damage the tissue architecture. To solve these issues, we have developed a biopsy removal module that seamlessly

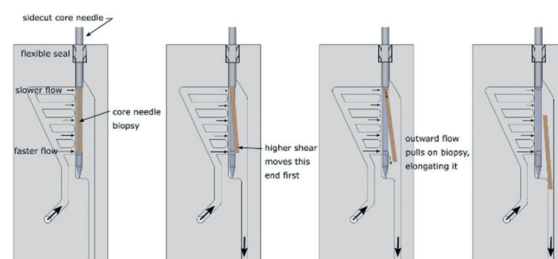


Fig. 1 Diagram of fluid mechanics involved in the removal of a CNB from a side-cut needle device using the 3D printed biopsy removal module. Successful removal results from the higher shear flow at the distal end of the CNB.

integrates into the CoreView chip. The biopsy removal module is designed to use one source flow, divided into an array of unequal-flow-resistance channels to spatially vary the amount of fluidic shear stress along the length of the biopsy over time (Fig. 1). It distributes the volumetric flow gradient using parallel rectangular channels two times longer at the proximal end of the biopsy than at the distal end. This flow gradient, in time, is designed to be highest at the distal end of the biopsy to ensure it is separated from the needle first. This design prevents the biopsy from folding upon itself and/or breaking, which can occur if the proximal end is separated first. The pulsatile, burst flow used to remove the biopsy comes from a “Hi-flow” PBS fluidic system, which provides a higher volumetric flow rate ($1\text{--}5\text{ mL s}^{-1}$ in $50+\text{ }\mu\text{s}$ pulses) than the transport pump (Fig. 2). This Hi-flow PBS pump is built using an air pump (KNF, Germany) and pressure regulator (SMC, USA) to pressurize a DURAN glass bottle filled with PBS (DWK Life Sciences, Shanghai). The biopsy removal module is designed to accompany most commonly used needle sizes (14–18-gauge) and ultimately moves the biopsy into the 2 mm-diameter main cylindrical channel for transport to the staining and imaging chamber.

Proof-of-concept device. Testing of the biopsy removal module was performed in two main stages: the proof-of-concept module (Fig. 1) and the integrated chip, based on the overall conceptual design shown in Fig. 3. For the proof-of-concept device, the biopsy removal module was 3D printed as its own part and connected directly to the Hi-flow PBS system of the CoreView millifluidic system. 10 mm 14-gauge side-cut CNBs (Mission, Bard Biopsy, USA) of breast ($N = 29$), kidney ($N = 21$), liver ($N = 40$), lung ($N = 25$), and lymph node ($N = 31$) were acquired from porcine organs that were resected post-euthanasia. These tissues were chosen because

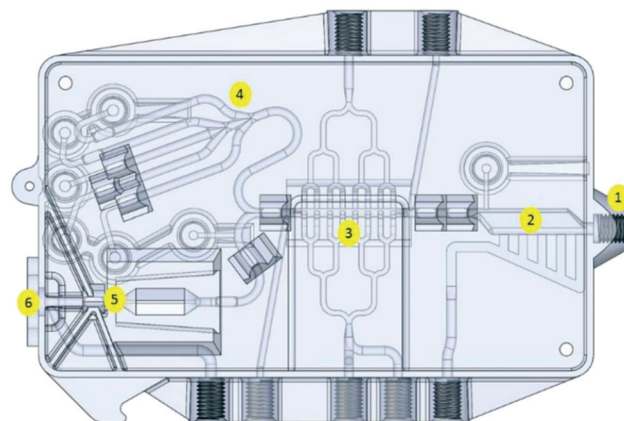


Fig. 3 CAD image of a conceptual end-product design of the CoreView chip. This model features (1) a port for needle insertion, (2) the biopsy removal module, (3) a chamber for staining and rinsing, biopsy rotation, and imaging, (4) the multiplexed storage “parking” module, (5) the biopsy segmentation module, and (6) an exit port for biopsy removal from the chip.

they are common organs for needle biopsies and each display unique mechanical characteristics that affect separation from the needle.^{9,10} PBS was flowed in three-pulse intervals driven by a bottle pressure that was incrementally increased until the biopsy was removed. For each biopsy, we recorded the tissue type, freshness, intactness (before and after removal), successful release, and the pressure at release.

Biopsy removal module in the CoreView chip. To test the performance of the biopsy removal module in the integrated chip, similar methods used to test the proof-of-concept device were performed. All CNBs were acquired from freshly resected porcine organs (20 each of breast, kidney, lung, and pancreas) using a 14-gauge, 22 mm side-cut needle (MaxCore, Bard Biopsy). To ensure the biopsy removal module works with varying needle sizes, similar testing was performed using 14, 16, and 18-gauge side-cut needles (MaxCore, Bard Biopsy) and porcine kidney.

Biopsy transport and storage

The CoreView chip relies on a single 2 mm-diameter cylindrical channel to transport the removed biopsy between modules. This transport is accomplished using pulsatile flow from a type 7615 micro-dosing fluidic pump (Burkert, USA) in small, $5\text{ }\mu\text{L}$ pulses with a short rise time. Directed transport can be performed using the micro-dosing pump in forward or reverse with at least one exit valve open (Fig. 2). Multiplexed storage of biopsies, referred to herein as biopsy “parking”, can be achieved by opening only the desired “parking space” valve until the biopsy is positioned in the chosen parking space channel, then closing that valve and opening another. The biopsy should not be able to leave that channel until the valve is opened again and fluid is driven in reverse. Biopsy parking may be ideal for in-chip fixation with formalin or other fixatives, which is required for many downstream diagnostic procedures.

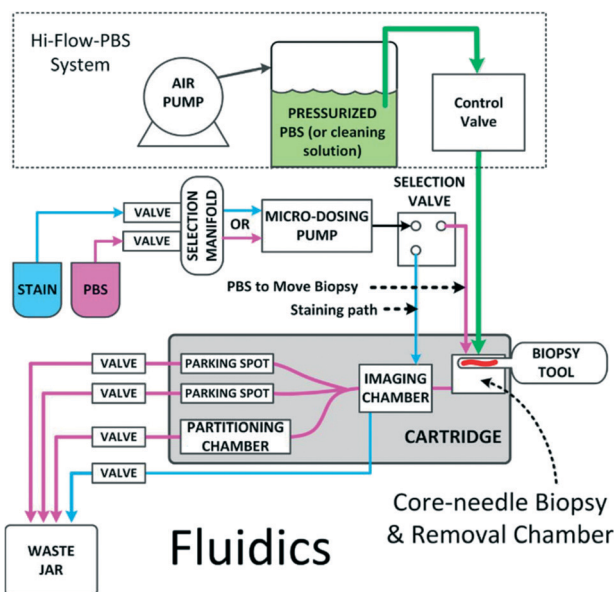


Fig. 2 Detailed diagram of the CoreView fluidics system with a simplified chip. All pumps and valves are controlled by LabVIEW with custom drive electronics and NIDAQs.

Biopsy staining and imaging

As a histopathologic device, the CoreView chip must demonstrate the ability to stain a CNB for enhanced optical image contrast. When flow rates less than those used in biopsy transport are employed, CNBs do not significantly move during staining and rinsing steps. In the CoreView chip, staining is performed in the imaging chamber using 50–75% smaller channels for stain inflow and outflow to limit biopsy movement. After staining and subsequent rinsing, imaging is performed using optical microscopy. To image the entire length of the CNB, a computer-controlled X–Y translational stage is used with optional Z-plane focus scanning for expanded depth-of-field. Full-biopsy panoramic images were mosaicked using MATLAB (MathWorks, USA) or ImageJ (NIH, USA).

With this paper, we present a video demonstration of the CoreView chip and millifluidics system (Movie S1† and Fig. 2–4). This video illustrates two clinical applications: (1) ROSE adequacy of a renal core biopsy that requires glomeruli counting, and (2) identifying tissue types and imaging nuclei on the surface of a breast CNB. The demonstrated features of this chip will be discussed in the “Results and discussion” section. The video frames shown in Fig. 4, captured from Movie S1,† illustrate the application of glomeruli counting using CoreView. A 20 mm 14-gauge porcine kidney CNB is shown undergoing insertion, removal, transport, and imaging using oblique LED illumination, a 4× objective, and color camera imaging in reflection (USB 3.0 xiD CCD Ximea Corp). The final panorama of the CNB, which is a mosaic of a series of color images, exemplifies future computer-aided detection of kidney glomeruli to enable remote pathology, enhanced with artificial intelligence in the future.

The image processing for generating the panorama was conducted in MATLAB R2020b (MathWorks) in the following steps: first, a Gaussian filter was applied to each image to remove noise and a threshold was then applied to remove the background signals (Fig. S1a and b†). Next, a contrast-limited adaptive histogram equalization (CLAHE) function was applied to each channel of the red, green, blue (RGB) color space and then the S channel of the hue, saturation, value (HSV) color space, was used to enhance the saturation of the image (Fig. S1c and d†).¹¹ After this step, the processed images were stitched using SURF and RANSAC features and the alpha blending method.^{12,13} Glomeruli detection for this image was achieved using a special weighted equation that employs RGB channel data and grayscale intensity, and an adaptive threshold based on regional intensity morphological operation (Fig. S1e and f†). Due to its relatively long processing time of 4.25 seconds per frame, and 17 seconds per mosaic, this glomeruli detection method has been superseded by a trained algorithm in ImageJ, explained later.

Also included in the video is ROSE adequacy imaging of a 20 mm 14-gauge porcine breast CNB (Mission, Bard Biopsy) using microscopy with ultraviolet surface excitation

(MUSE) imaging. MUSE uses deep-ultraviolet (DUV) LEDs to excite the first 10–20 μm of tissue, allowing for the imaging of only the first few layers of cells.¹⁴ Prior to imaging, the breast CNB was stained in under 1 minute with 5 μg mL^{−1} Hoechst 33342 (Thermo Fisher Scientific, USA) in PBS added to 10 μg mL^{−1} rhodamine B (Thermo Fisher Scientific) in PBS. Hoechst is a nuclear stain that emits blue light and rhodamine B is a cytoplasmic stain that emits reddish orange light when excited with 285 nm DUV light. Images were viewed and saved using Ximea CamTool (Ximea Corp.).

Biopsy tracking algorithm development

For transitioning from manual control to computer automation, we have developed a camera-based biopsy tracking algorithm in MATLAB R2020b (MathWorks). This algorithm was developed and used on a 16G RAM PC desktop with a Ryzen 3600XT processor (AMD, USA) and a GeForce GTX 1660 Ti graphics card (Nvidia, USA). To develop the algorithm, 14-gauge porcine kidney CNBs were acquired and input into the CoreView chip and transported throughout the channels. The chip was backlit using a bank of white LEDs under a plastic white diffuser and videos were taken using a color video camera (MOKOSE 4K, Shenzhen Yunlang Technology Co., China). In all the following implementations of camera tracking, temporal frequency of the video camera was 10 Hz or greater, which limited the speed of the feedback control.

Identifying the biopsy in each frame (frame tracking). The main targets of the algorithm are the biopsy and its possible fragments. Due to variable illumination, the color and saturation of the biopsy is not constant during transport. As a result, the algorithm must be insensitive to environmental changes. To create this algorithm, we first compared the mean intensity values of each channel in the RGB color space of a biopsy, the transport solution, and the background of a single frame (Table S1†). This comparison revealed that $(R - G) + (R - B)$ is the most significant distinguishing value between the three components. After performing this channel operation, the image was transferred into a binary image using MATLAB's `imbinarize()` function with a threshold of 0.47.¹⁵ After binarizing, the image was morphologically opened using MATLAB's `imopen()` function to decrease the noise and make regions more distinct. Small fragments that are irrelevant to successful CoreView function may exist and create identifiable regions in this step. These regions, which are smaller than 1000 sq. pixels, are simply removed after this step to prevent tracking. A green rectangle was generated onto the frame around the identified biopsy using a bounding box and centroid determined using MATLAB's `regionprops()` function.

Multiple object tracking using tracks (video tracking). Some tissues may undergo significant fragmentation during removal and transport. Furthermore, air may be present in the needle, creating gas bubbles upon biopsy removal. To

account for the tracking and indexing of multiple objects at once, each detected object was assigned a track that is maintained between frames. Each track was assigned the area, bounding box, and centroid properties of the distributed region using MATLAB's `regionprops()` function. Before tracks were assigned or modified, detections are made by the algorithm using a tracking function that finds the difference between the current frame and the last frame and applies the previously described frame tracking algorithm. To determine which track detections were being assigned to, we employed an area difference matrix defined as:

$$AD_{ij} = |\text{Track Area}_i - \text{Detection Area}_j|$$

where i is the index of tracks and j is the index of detections. The track with the least area difference, identified by the above matrix, was used to assign detections (Fig. S2†). If more tracks were created in a previous frame than detections that existed in the current frame, *i.e.*, the fragments were compressed together, at least one track must be deleted for simplicity. The same area difference matrix track assignment method is used, but the track(s) with the largest area difference are removed.

In the RGB space, the tracking algorithm cannot reliably distinguish bubbles from the background. It is important to identify any bubbles that exist in the chip because they add compliance to the fluidic system, preventing optimal and consistent transport flow profiles, and can also be indistinguishable from tissue by photosensors. As this detection is infeasible using the RGB space, the frame must be transferred into the HSV color space. While the background varies in this space due to location and/or lighting, a single bubble does not (Table S2†). With this improvement, the same frame tracking and video tracking

algorithms were used to detect any tissue, in the RGB color space, and gas bubbles in the HSV color space, in the chip. To distinguish from the biopsy, bubbles were indicated using solid red circles instead of green bounding boxes. A flow chart of the full biopsy and bubble tracking algorithm can be seen in Fig. S3†.

Glomeruli detection and counting with ImageJ

To provide immediate glomeruli counting at the point-of-care, we have adapted a blob detection technique¹⁶ to identify and count all the glomeruli in each image acquired with CoreView. First, the raw image (Fig. 5a), taken using white light reflectance microscopy, was edited using photo processing software [Topaz Labs] to increase contrast and enhance edges (Fig. 5b). Next, the edited image was classified into potential regions of glomeruli using a trained Weka segmentation plugin in ImageJ¹⁷ (Fig. 5c). Once classified, the image was transformed into a black and white binary mask, and open, close, and fill holes operations were performed using their respective functions in the “Binary” options of ImageJ's “Process” tab. Lastly, glomeruli were detected, highlighted, and counted using ImageJ's “Analyze Particles” function (Fig. 5d). Non-glomeruli particles were excluded by ignoring small particles.

To evaluate the correlative accuracy of our glomeruli detection method, the results were compared to a pathologist's interpretation of the raw images. For this analysis, both the pathologist and the ImageJ operator were blinded to the other's results, and only the number of glomeruli were compared. For an adequate assessment, 10 total images from 4 different biopsies, all taken in one sitting to avoid environmental discrepancies, were used.

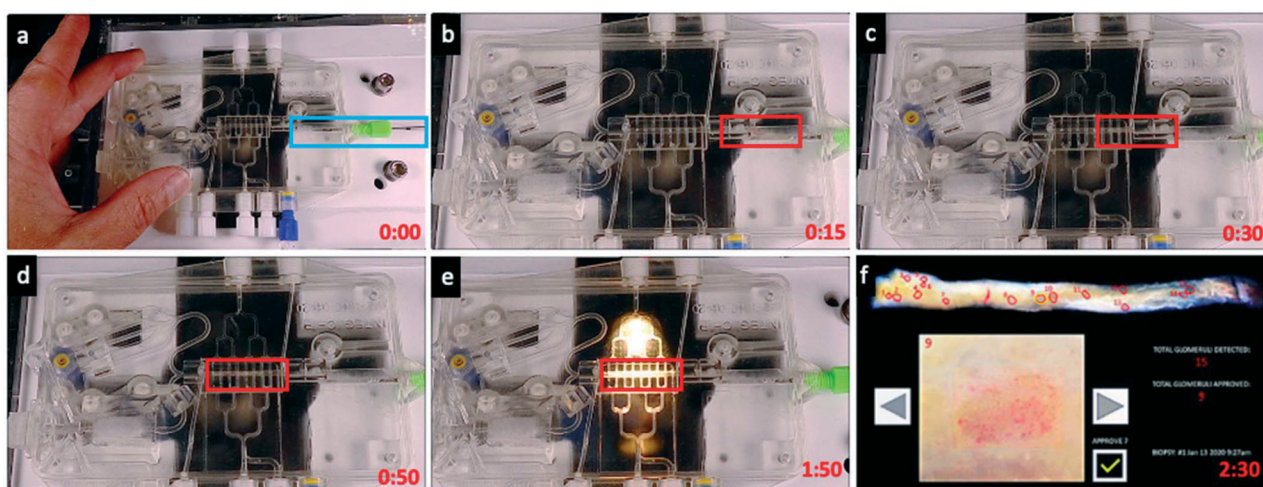


Fig. 4 A sequence of video frames from Movie S1† illustrating the entire process in the CoreView chip, including (a) needle insertion, (b) biopsy removal, (c) biopsy transport, (d) centering in imaging chamber with optional staining, (e) imaging, and (f) detection of glomeruli in a stitched series of CNB images. The red boxes outline the CNB, and the blue box outlines the inserted needle. Red numbers indicate the lapsed time (MIN: SEC) to detect the glomeruli from needle insertion. The example tele-pathology interface (f) is what the remote pathologist uses to read and count glomeruli or monitors the CoreView system with deep learning.

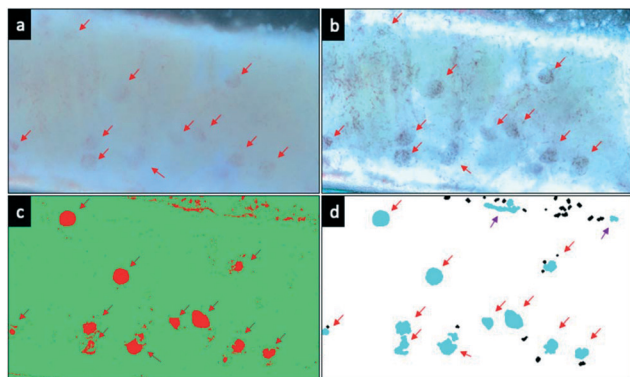


Fig. 5 An example of glomeruli detection using CoreView with red arrows pointing to glomeruli. (a) The raw image of a fresh porcine renal CNB. (b) The edited version of (a) to make glomeruli more detectable. (c) The trained Weka segmentation of (b), identifying possible glomeruli in red and non-glomeruli in green. (d) Final glomeruli detection (cyan) using ImageJ's "Analyze Particles" function. Purple up-arrows point to non-glomeruli details identified as glomeruli.

Biopsy segmentation proof-of-concept device

On-chip biopsy tissue segmentation, or partitioning, would be a valuable addition to the CoreView chip because it would enable multiple downstream diagnostic tests from one biopsy and allow for the sampling of a single identified tumorous or glomeruli-dense region from a CNB. To perform such a task, we require a module that can repeatedly target and cleanly cut a specific location along the biopsy. To achieve this operation, we designed for minimal fluid flow around the biopsy to prevent motion, a sharp cutting device, and a clear optical window to monitor segmentation. A proof-of-concept biopsy segmentation device was 3D printed, as described previously, to test various blade forces and trajectories as well as cutting channel geometries (Fig. 6). The device used

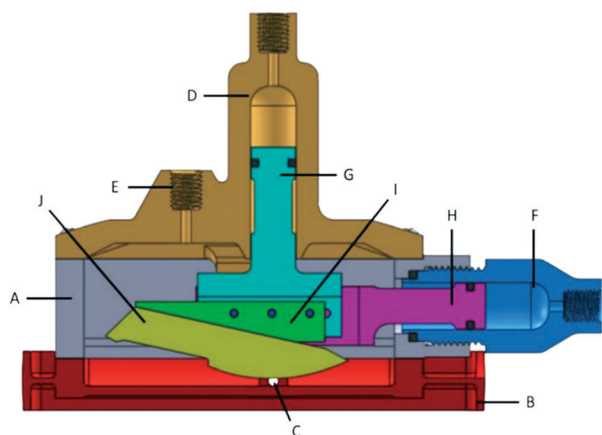


Fig. 6 CAD cross-section of the 3D printed biopsy segmentation proof-of-concept device colored and labeled to show individual parts. The device uses hydraulic cylinders (D and F) to vertically and horizontally move a blade (J) across the channel (C). Other components include the housing box (A), fluidic chip (B), supplemental fluid port (E), pistons (G and H), and blade holder (I).

conventional rigid hydraulic cylinder design practices and allowed the transport channel section to be interchanged to test variations of the channel-blade interface without printing multiple iterations.

Assembly of components. The biopsy segmentation proof-of-concept device consisted of seven 3D printed parts, all finish machined to tight tolerances ($\pm 12 \mu\text{m}$) with micro-grain carbide tooling on a manual lathe. The first component of the device was a housing box (Fig. 6A) sealed onto a fluidic chip (B) with a cutting chamber (C) using and a silicone gasket. The opposite side of the housing box was sealed onto a vertical actuating cylinder component (D) in the same manner. This component also acted as a top cover and contained a supplemental fluid port (E) for fluid displaced during actuation and air bubble purging. Both the housing box and the vertical cylinder cover were built with guides to constrain the motion of the pistons to a single direction. The horizontal cylinder (F) threaded into the right side of the housing box to allow for the installment of the internal moving components and was sealed with a dash 013 square profile O-ring. Each actuator contained its own piston (G and H), sealed with dash 010 double X-profile O-rings fitted to precision machined grooves in the pistons, that were designed with slots to guide the blade holder (I) *via* stainless-steel dowel pins. This guided movement moves a stainless-steel #23 scalpel blade (J), which is adhered to the blade holder with epoxy. The blade was intended to have a high ratio of horizontal sliding to vertical descending movement. During operation, the entire device was filled with PBS.

Testing the biopsy segmentation device. Two different cutting chambers were designed and tested (Fig. 7). The first and most simple design was a slotted cutting chamber, which had a horizontal gap in the channel to house the blade and a circular cut-out for post-segmentation biopsy separation *via* fluid flow. The second design was an elastomeric buffer cutting chamber, which had a similar horizontal gap and circular cut-out, but a large portion of the channel was open for the placement of a 3D printed elastomeric buffer. This buffer was very elastic, allowing the cut to close after the blade retracts. Both designs were tested for successful biopsy segmentation and separation using biopsies from a 14-gauge, 22 mm CNB gun (MaxCore, Bard

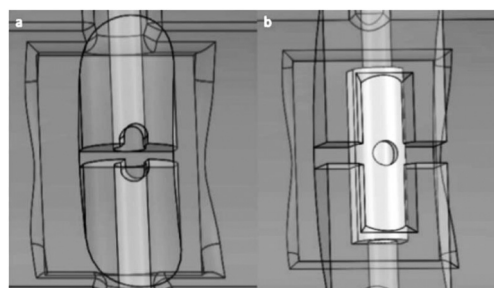


Fig. 7 CAD image of the (a) slotted cutting chamber and (b) elastomeric buffer cutting chamber of the 3D printed biopsy segmentation proof-of-concept device.

Biopsy). Both designs were connected to the CoreView millifluidics system *via* the transport pump and stain waste valves. They were also connected to the biopsy removal proof-of-concept device for easy biopsy removal and input into the tubing. The slotted cutting chamber device was tested with 6 porcine kidney CNBs and relied on manual control of the hydraulic cylinders *via* PBS-filled syringes. The needle was manipulated vertically and horizontally until the biopsy was successfully cut, and observations were recorded. The elastomeric buffer cutting chamber device was tested with CNBs of fresh porcine breast ($N = 3$), kidney ($N = 7$), and pancreas ($N = 6$) tissue. These tissues have very different mechanical properties, which enable the assessment of the robustness of the proof-of-concept device.^{8,9} Similar methods were used to manipulate the blade, and the number of passes along with any observations were recorded.

Results and discussion

Our histopathology lab on a chip millifluidic system, named CoreView, is centered around a clear chip that allows for the self-containment and automation of all biopsy handling and processing steps of histopathology (Fig. 3). This chip is designed to be mass-produced by injection molding but is currently 3D printed as single prototypes. The CoreView chip is also designed to be disposable but can be sterilized or ultra-cleaned with high-level disinfection processes used for endoscope reprocessing. Millifluidics is preferred to microfluidics for histopathology because it preserves tissue architecture and allows for optical imaging of both diseased cells and their microenvironment. A schematic of the entire millifluidic system prototype can be seen in Fig. 2. We have demonstrated that our CoreView chip successfully uses millifluidics to remove, transport, stain, image, and park needle biopsies (Movie S1†).

Biopsy removal from its needle

Results from the biopsy removal experiments are presented in Tables 1–3 and S3 and S4.† These results show that successful biopsy removal using the proof-of-concept device and the integrated chip module is efficient and reproducible across a wide range of tissues. Most importantly, our biopsy removal module allows for the visual assessment of an intact CNB with CoreView, which is not possible with other ROSE techniques. In the proof-of-concept module experiment, most

Table 2 Biopsy removal efficiency in the integrated CoreView chip using 14 g side-cut needle biopsies

| Tissue | Removed from needle | Biopsy stayed intact | Removal pressures (psi) | | |
|----------|---------------------|----------------------|-------------------------|--------|-----------|
| | | | Mean | Median | Std. Dev. |
| Breast | 100% | 90% | 3.5 | 3.0 | 1.9 |
| Kidney | 100% | 100% | 2.4 | 2.0 | 0.8 |
| Lung | 100% | 95% | 3.1 | 3.0 | 1.2 |
| Pancreas | 100% | 94% | 3.5 | 2.0 | 2.3 |

CNBs were fully released, but only 84% of lung CNBs were removed while 100% were removed in the integrated chip (Tables 1 and 2). The most likely reason for this difference, and differences in other organs, is the freshness of the sample. Fresh tissue is found to change material properties within hours of resection.¹⁸ In the proof-of-concept module experiments, the tissue was either fresh (used within five hours of resection) or refrigerated (for 19+ hours after resection), while the integrated chip experiments only used fresh tissue. Differences in adhesion to surfaces (“stickiness”), elasticity, and the tendency to break into fragments are very pronounced between these post-resection times. As a result, the ability of a CNB to be removed and stay intact is highly dependent on time since resection (time *ex vivo*).

The experiments assessing the range of side-cut needle sizes showed that the biopsy removal module can remove all CNBs, ranging from 14- to 18-gauge, with low pressure flow (Table 3). This preliminary data indicates that higher gauge (smaller diameter) needles may require a higher driving pressure to remove the biopsy, but the sample size is too small to draw significant conclusions. The biopsy removal module can also be used to pull a CNB from end-cut needles with assistance from a central wire or stylet running out through the needle tip during fluidic flow. Minor channel-size modifications will be needed to accept bigger diameter needles, such as 9–12-gauge used for larger breast tumors.

The integrated chip biopsy removal experiments show that the bottle pressure of the high-flow PBS can be lower than originally estimated to be necessary by the concept module experiments. Utilizing this result to modify the Hi-flow PBS system will prevent excessive PBS waste and help to reduce a CNB “overshoot” of the staining/imaging compartment if it is released in the first couple pulses. Although these results are

Table 1 Biopsy removal efficiency using the 3D printed biopsy removal proof-of-concept module containing 14 g side-cut needle biopsies

| Tissue | N | Removed from needle | Biopsy stayed intact | Removal pressures (psi) | | |
|------------|----|---------------------|----------------------|-------------------------|--------|-----------|
| | | | | Mean | Median | Std. Dev. |
| Breast | 29 | 90% | 76% | 7.1 | 3.5 | 7.2 |
| Kidney | 21 | 100% | 76% | 3.4 | 2.0 | 5.0 |
| Liver | 40 | 98% | 68% | 4.0 | 2.0 | 4.1 |
| Lung | 25 | 84% | 96% | 9.0 | 10.0 | 7.8 |
| Lymph node | 31 | 97% | 77% | 4.4 | 2.0 | 3.8 |

Table 3 Biopsy removal efficiency of various side-cutting needle sizes in the integrated CoreView chip. All CNBs were resected from porcine kidney refrigerated for 21 days

| Needle gauge | N | Removed from needle | Biopsy stayed intact | Removal pressures (psi) | | |
|--------------|----|---------------------|----------------------|-------------------------|--------|-----------|
| | | | | Mean | Median | Std. Dev. |
| 14 | 10 | 100% | 100% | 3.6 | 3.0 | 2.1 |
| 16 | 10 | 100% | 100% | 3.2 | 3.0 | 1.4 |
| 18 | 10 | 100% | 80% | 5.4 | 5.0 | 2.7 |

very promising, around 5% of CNBs may fragment during removal, depending on the quality and composition of the biopsy. Fragmentation can cause challenges in biopsy tracking and make it harder to accumulate all tissue in the imaging chamber. To overcome these challenges, a new module containing an in-line sifter or sieve can be used to amass all the fragments into a smaller volume which can be transported back into the imaging chamber as a single packet.

Biopsy transport, staining, and imaging

We have shown that the CoreView millifluidic histopathology on a chip can successfully and reliably transport, stain, and image core needle biopsies (Movie S1†). Furthermore, we have demonstrated that reliable bidirectional fluid transport can be achieved with 0.5 mm positioning accuracy. Full operation of two current prototypes can be seen in Movie S1.† The first prototype chip used in the video (Fig. 3) shows successful removal, transport, and parking of a fresh porcine kidney CNB using system millifluidics. This biopsy is imaged using oblique reflectance for the computer-aided detection of low-contrast glomeruli found in diseased or transplanted kidney tissue (Fig. 4). The image processing of the CNB provides higher contrast than white-light imaging used in a pathologist's portable inspection scope. Furthermore, pathologists at remote sites could inspect CoreView images and confirm kidney glomeruli counts within minutes of tissue acquisition, reducing patient and clinician wait times.

The second prototype chip used in the video shows bidirectional transport and staining of a fresh porcine breast CNB using CoreView millifluidics. Note that, during the accelerated, 1 minute staining and rinsing portion of Movie S1,† a large air bubble was introduced with the staining solution. This air bubble adhered to the biopsy, adding compliance and surface tension, resulting in atypical movement of the biopsy during the lower staining and rinsing pulsatile flows. By adequately priming the system prior to needle insertion, gas introduction into the system can be prevented.

After tissue staining and rinsing, MUSE imaging of the CNB revealed nuclei on the tissue surface. MUSE imaging is under development for the rapid, high quality diagnostic assessment of breast tissue.¹⁹ While MUSE is not yet commercially available, the technique provides excellent synergies with the ROSE adequacy capabilities of our system. Images produced using MUSE, such as the ones displayed in this section of the video, may be used to identify and quantify tumor-containing regions in CNBs. However, image quality is not sufficient at low magnification to reliably make confident diagnoses, and the lack of tissue compression against the imaging window in this initial prototype is a significant source of artifacts.²⁰

Although Movie S1† shows the successful demonstration of a nearly completed CoreView chip and millifluidic system, the device is still not complete. Firstly, operation is not yet

fully automated, with the exception of the LABVIEW interface that controls and monitors all pumps, valves, and sensors. As a result, each millifluidic pulse, or series of pulses, is controlled by the operator. Multiple systems have been developed, or are still under development, to enable CoreView automation, including the real-time biopsy tracking algorithm. The final chip will likely feature a linear lens and phototransistor after the biopsy removal module to turn off the high-flow pump more quickly than the biopsy tracking algorithm can. This feature will prevent any biopsy overshoot of the staining chamber.

Biopsy tracking

The complete biopsy tracking algorithm successfully identified and tagged all biopsies, biopsy fragments, and bubbles on all videos. The detection of a biopsy in the RGB color space is shown in Fig. S4† and the detection of an air bubble in the HSV color space is shown in Fig. S5.† The final result of biopsy and bubble tracking is shown in Fig. 8 and Movie S2.† Different illumination conditions were also used in many of the videos, but no change in tracking performance was perceived. This is an important quality for the clinical application of the CoreView system, especially in the developing world, where the point-of-care may not be in a hospital or clinic. A robust biopsy tracking algorithm is necessary for the automation of the CoreView system because no two needle biopsies have the exact same properties. Different biopsies may not be removed from the needle nor transported at the same rates, which means that we cannot expect a fixed number of pulses for transport from the needle to the staining and imaging chamber to work for all CNBs.

While this algorithm is intended to be used for real-time tracking to guide system automation, its current form is limited to a speed of around 9–10 frames-per-second (fps) while the videos used had a frame rate of 25 fps. This limitation may be remedied by resizing each frame into a lower resolution image, increasing computational resources, or reprogramming into more rapidly executable algorithms.

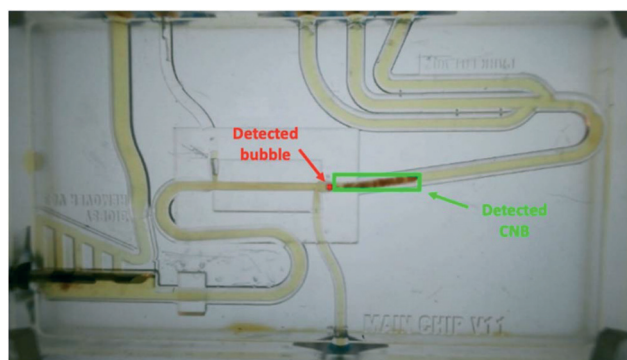


Fig. 8 Result of the biopsy and gas bubble detection algorithm. This image is of one frame of a video showing the transport of a 14 g, 20 mm-long porcine kidney CNB (green box) and a lone bubble (red circle).

Additionally, the algorithm speed can be greatly improved by restricting the detection window to the CoreView chip fluidic channels, but current prototyping makes the immediate implementation of this change infeasible. Spatial resolution of the camera tracking is limited to 0.53 mm which matches the minimum step size of the pulsatile fluidic pump used for bidirectional biopsy movement.

Glomeruli detection and counting with ImageJ

To confirm the correlative accuracy of our glomeruli detection method in ImageJ, we compared the counts to the number of glomeruli identified by a trained pathologist in the raw images. This comparison revealed that our method detected a median absolute difference of +2 glomeruli per image than the pathologist. While this may result from glomeruli undetectable without computer enhancement, we believe that this difference is purely coincidental. For example, in the blinded review of the renal CNB displayed in Fig. 5, the pathologist determined there were 13 glomeruli present while our detection method identified 15 possible glomeruli. The extra 2 identified particles were present in tissue artifacts outside the boundaries of the biopsy (Fig. 5d purple up-arrows). Future repeated imaging in CoreView chips will allow more sophisticated training with deep learning from trained pathologists and nephrologists that is expected to improve this correlation with automated glomeruli counting.

With a processing time of <1 second per image, our glomeruli detection method can identify, count, and display the number of glomeruli present in one field-of-view of a renal biopsy before repositioning the mechanical stage and acquiring the next image. As a result, this method can deliver immediate detection in the CoreView system at the point-of-care, revealing valuable information necessary to prevent additional biopsy procurement. Additionally, glomeruli detection, and the resulting biopsy segmentation to separate certain numbers of glomeruli for different downstream tests, with CoreView is likely to save pathologists up to one hour of time typically spent traveling to receive, and occasionally waiting for, the biopsy and performing glomeruli identification triage for three downstream tests.

Biopsy segmentation

Biopsy segmentation was performed as shown in Fig. 9. Both proof-of-concept biopsy segmentation devices were able to successfully cut the tested CNBs, but each device had its own limitations.

The slotted cutting chamber device showed consistent cutting performance after multiple passes across the biopsies with minimal tissue snagging during transport due to its relatively simple geometry. Multiple passes were required to produce cutting forces high enough to completely cut the biopsies yet low enough to avoid pulling the tissue into the device through the cut-out. The tendency to inadvertently pull biopsies out of the channel could be remedied by

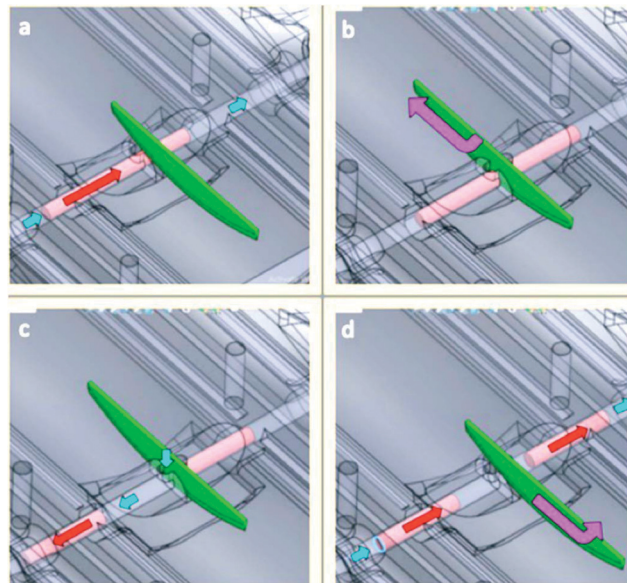


Fig. 9 A series of CAD images showing the intended blade movements of the biopsy segmentation proof-of-concept device. (a) Placement of the CNB (blush red) using transport millifluidics prior to blade (green) movement. (b) Slicing (pink) with the blade. (c) Pushing the biopsy away from the blade using inflow (cyan) through the circular cut-out. (d) Blade retraction and biopsy transport.

decreasing the clearance between the blade and the cut-out or by adding a moving component, such as an elastomeric buffer, at the cost of manufacturing complexity, to provide a zero-clearance fit.

The elastomeric buffer cutting chamber device houses the biopsy in an elastic sheath that is cut with the biopsy. This design constrained the lateral motion of the biopsy near the blade more efficiently than the slotted cutting chamber and allowed for the higher cutting forces needed to cut the tissue in one or two passes (Fig. S6†). However, the softer and more fibrous breast biopsies were frequently snagged between the buffer and the channel, prior to entering the buffer, and at the buffer's pinch point after the blade was retracted.

Overall, these experiments show that successful biopsy segmentation using fluidics is possible and has the potential to be integrated into a CoreView chip. However, these proof-of-concept devices are over-sized and inordinately complex. The final module will likely employ fewer, simpler, and less costly parts with compliant devices such as diaphragms, bending actuators using differential stiffness, or extending bellows.²¹ A channel design that allows the biopsy to be cut with simple 1D motion will further simplify this mechanism. Exact components will be determined with future iterations and experiments.

Implications for the future of pathology

CoreView demonstrates the potential to overcome many limitations associated with small needle biopsy

histopathology. Firstly, the ability to use millifluidics to automatically remove intact tissue from a biopsy needle, and then reliably transport, stain, image, store, and segment biopsies can alleviate many problems associated with manually handling biohazardous human tissue specimens, stains, and fixatives. Automating biopsy handling also allows for non-destructive tissue preservation from needle procurement to imaging and later fixation. Seamless tissue procurement and non-destructive tissue handling with CoreView would be major improvements over standard ROSE protocols that are limited to cytological analysis. Secondly, preserving fresh tissue after initial assessment enables sample preparation of several downstream diagnostic tests, including RNA integrity number (RIN) for gene expression analysis, and other ‘-omics’ analyses. Formalin fixation disrupts DNA, RNA, and other biologic macromolecules, affecting molecular analyses that can guide personalized cancer therapies.²² Using the segmentation module to divide a sample, and the parking module to hold the valuable tissue, allows for tissue fixation and/or preservation with different solutions. For example, one renal biopsy could be divided after CoreView imaging into segments which could then be separately fixed in formalin for conventional histopathology, chemical preservative for electron microscopy, and PBS for future immunofluorescence imaging. CoreView also has the potential to monitor tissue fixation using a novel non-contact module. This 3D-printed low-cost monitor measures the optical transmittance of a CNB in a millifluidic chamber and can be used to determine when the biopsy is optimally formalin-fixed.²³ In the future, additional microfluidic modules can be added to the CoreView millifluidic chip for maintaining viability of fresh tissue for real-time chemical monitoring, reactions to applied chemotherapy drugs, and analysis of extracted analytes from CNBs.^{24–26}

The ability of CoreView to produce histopathologic images in minutes at the point of care, instead of hours to days in a remote laboratory, may be especially helpful in low resource settings. Breast cancer is the most common cancer and second-leading cause of cancer-related deaths in Sub-Saharan Africa.²⁷ Standard CNB histopathology requires specialized equipment and laboratories, which are available in fewer than 10% of hospitals in resource-limited countries.²⁸ Additionally, skilled laboratory personnel are scarce in these regions. For example, Africa has 100-fold fewer pathologists *per capita* than the US and Canada.^{28,29} A lower-cost and portable CoreView system using MUSE or other emerging thick-tissue imaging techniques could be used to provide same-day therapeutic decision making in settings where follow-up appointments for affected patients may be unattainable.³⁰

Conclusions

In this paper, we present the current state of CoreView, our novel millifluidic histopathology lab-on-a-chip device that

handles fresh core needle biopsies from acquisition to imaging. We demonstrate that pulsatile millifluidics can be used to reliably remove CNBs from side-cut needles (14–18-gauge), transport CNBs through a 2 mm channel with 0.5 mm positioning accuracy, and stain and rinse stationary CNBs. We also confirm that fluidics can be used to cut fresh CNBs into multiple segments for separate downstream diagnostics. Lastly, we show that a real-time biopsy tracking algorithm can be employed to enable system automation using machine vision. Using the current low-resolution optical microscopy in this initial report, the CoreView system can perform ROSE assessment within a few minutes of biopsy acquisition to ensure tissue adequacy for diagnostics. Combining the CoreView system with telepathology, such as with kidney glomerular assessment, would allow remote sample evaluation by pathologists, reducing the need for the pathologist to travel to the radiology suite and streamlining patient care. Point-of-care tissue adequacy assessment would also reduce patient risk and discomfort by reducing the need for additional biopsies. In combination with emerging high-resolution fresh tissue microscopies, CoreView point-of-care tissue diagnosis could also facilitate more rapid therapeutic decision making, especially in low resource settings.

Conflicts of interest

Most authors participate in the royalty sharing program at the University of Washington, which owns CoreView patent filings. EJS is also a shareholder in ROSEbiopsy Inc., which also owns some CoreView patents.

Acknowledgements

Funding provided by the University of Washington CoMotion Innovation Fund, the Washington Research Foundation (Phase 1 Award and Undergraduate Research Fellowship), and the National Cancer Institute Exploratory R21 CA 246359 award. We thank Shawn Swanson for loaning us his personal form 3 printer. We thank Yak-Nam Wang PhD from the University of Washington for providing fresh discarded pig tissues. We thank Rodney Schmidt, MD, for his initial mentorship of CoreView from a pathologist's perspective.

Notes and references

- 1 M. Titford, *J. Histotechnol.*, 2006, **29**, 99.
- 2 K. P. H. Pritzker and H. J. Nieminen, *Arch. Pathol. Lab. Med.*, 2019, **143**, 1399.
- 3 P. A. VanderLaan, *Cancer*, 2016, **124**, 862.
- 4 S. Satturwar, N. Rekhtman, O. Lin and L. Pantanowitz, *Cytopathology*, 2020, **9**, 322.
- 5 W. L. Whittier, C. Gashti, S. Saltzberg and S. Korbet, *Clin. Kidney J.*, 2018, **11**, 616.
- 6 K. A. Shaikh, K. S. Ryu, E. D. Goluch, J. Nam, J. Liu, C. S. Thaxton, T. N. Chiesl, A. E. Barron, Y. Lu, C. A. Mirkin and C. Liu, *Proc. Natl. Acad. Sci. U. S. A.*, 2005, **102**, 9745.

- 7 K. C. Bhargava, B. Thompson and N. Malmstadt, *Proc. Natl. Acad. Sci. U. S. A.*, 2014, **111**, 15013.
- 8 S. You, Y. Sun, E. J. Chaney, Y. Zhao, J. Chen, S. A. Boppart and H. Tu, *Biomed. Opt. Express*, 2018, **9**, 5240.
- 9 J. Rosen, J. D. Brown, S. De, M. Sinanan and B. Hannaford, *J. Biomech. Eng.*, 2008, **130**, 021020.
- 10 A. W. Hudnut, B. Babaei, S. Liu, B. K. Larson, S. M. Mumenthaler and A. M. Armani, *Biomed. Opt. Express*, 2017, **8**, 4663.
- 11 K. Zuiderveld, *Graphic Gems IV*, Academic Press Professional, San Diego, 1994.
- 12 H. Bay, T. Tuytelaars and L. Van Gool, *SURF: Speeded Up Robust Features*, Springer, Berlin, Heidelberg, 2006.
- 13 M. A. Fischler and R. C. Bolles, Random sample consensus: A paradigm for model fitting with applications to image analysis and automated cartography, *Commun. ACM*, 1981, **24**(6), 381–395.
- 14 F. Fereidouni, Z. T. Harmany, M. Tian, A. Todd, J. A. Kintner, J. D. McPherson, A. D. Borowsky, J. Bishop, M. Lechpammer, S. G. Demos and R. Levenson, *Nat. Biomed. Eng.*, 2017, **1**, 957.
- 15 MathWorks Help Center, <https://www.mathworks.com/help/index.html>, (Apr. 20, 2021).
- 16 P. McMillan, Fundamentals of Image Quantification, https://microscopy.unimelb.edu.au/__data/assets/pdf_file/0007/2010022/Fundamentals-of-image-quantification-sml.pdf, (Dec 4, 2021).
- 17 Trainable Weka Segmentation, <https://imagej.net/plugins/tws/>, (Dec 4, 2021).
- 18 H. Nitta, B. D. Kelly, C. Allred, S. Jewell, P. Banks, E. Dennis and T. M. Grogan, *Pathol. Int.*, 2016, **66**, 313.
- 19 W. Xie, Y. Chen, Y. Wang, L. Wei, C. Yin, A. Glaser, M. Fauver, E. Seibel, S. Dintzis, J. Vaughan, N. Reder and J. Liu, *J. Biomed. Opt.*, 2019, **24**, 026501.
- 20 F. J. Voskuil, J. Vonk, B. van der Vegt, S. Kruijff, V. Ntziachristos, P. J. van der Zaag, M. J. H. Witjies and G. M. van Dam, *Nature Biomedical Engineering*, 2021, pre-print.
- 21 K. Ogura, S. Wakimoto, K. Suzumori and Y. Nishioka, *Micro pneumatic curling actuator – Nematode actuator*, *IEEE International Conference on Robotics and Biomimetics*, 2008.
- 22 A. Frankel, *Aust. N. Z. J. Surg.*, 2012, **82**, 395.
- 23 S. Lim, *PhD dissertation, Mechanical Engineering*, University of Washington, Seattle, WA, 2020.
- 24 L. T. Cheah, Y. H. Dou, A. M. L. Seymour, C. E. Dyer, S. J. Haswell, J. D. Wadhawan and J. Greenman, *Lab Chip*, 2010, **10**, 2720.
- 25 L. F. Horowitz, A. D. Rodriguez, T. Ray and A. Folch, *Microsyst. Nanoeng.*, 2020, **6**.
- 26 S. Abdulwahab, A. H. C. Ng, M. D. Chamberlain, H. Ahmado, L. A. Behan, H. Goma, R. F. Casper and A. R. Wheeler, *Lab Chip*, 2017, **17**, 1594.
- 27 *The Cancer Atlas*, <https://canceratlas.cancer.org/the-burden/sub-saharan-africa/>, 2021.
- 28 African Strategies for Advancing Pathology, http://www.pathologyinafrica.org/surveydata/map-data.php?type=n_path%7Cmin-max%7C1%7C1%7C1%7CNumber+of+Pathologists+Per+Million+Population#, (May 23, 2021).
- 29 D. M. Metter, T. J. Colgan, S. T. Leung, C. F. Timmons and J. Y. Park, *JAMA Netw. Open*, 2019, **2**, e194337.
- 30 R. Levenson, F. Fereidouni and T. Morningstar, *Lab. Invest.*, 2021, vol. 101.